

Velocity Distribution of Dark Matter Spike around Schwarzschild Black Holes and Effects on Gravitational Waves from EMRIs

ZI-CHANG ZHANG¹ AND YONG TANG^{1, 2, 3, 4}

¹*School of Astronomy and Space Science,
University of Chinese Academy of Sciences (UCAS), Beijing 100049, China*

²*School of Fundamental Physics and Mathematical Sciences,
Hangzhou Institute for Advanced Study, UCAS, Hangzhou 310024, China*

³*International Center for Theoretical Physics Asia-Pacific, Beijing/Hangzhou, China*

⁴*National Astronomical Observatories, Chinese Academy of Sciences, Beijing 100101, China*

ABSTRACT

Dark matter (DM) constitutes the predominant portion of matter in our universe. Despite compelling evidence, the precise characteristics of DM remain elusive. Among the leading DM candidates are weakly interacting massive particles, which may aggregate into steep concentrations around the central black holes of galaxies, forming dense spikes. Employing Schwarzschild geometry, we assess the density and velocity distribution of DM within such spikes. Through variations in black hole masses and dark halo parameters, we identify universal features in the density profile of DM and fit them with Gaussian distributions. Additionally, we investigate the impact of dynamical friction on gravitational waves (GWs) generated by extreme-mass-ratio inspirals (EMRIs) within DM spikes. Our findings uncover phase shifts in the time-domain waveform, potentially providing significant insights for the GW-based detection of DM in galactic centers.

Keywords: Dark Matter — Black Hole — Gravitational Wave

1. INTRODUCTION

Various observational evidence suggests that DM constitutes a substantial component of the universe, including galactic rotational curves, colliding bullet cluster, gravitational lensing, large-scale structure, and anisotropy in cosmic microwave background. However, the exact nature of DM is still unknown. One leading paradigm suggests that DM might be weakly-interacting massive particles (WIMPs), which have been searched on particle colliders, directly with scattering with atoms, and indirectly by annihilation relic in astrophysical environments (Bertone et al. 2005; IBARRA et al. 2013; Schumann 2019). And the latter two methods depends on DM density profile.

To describe the density distribution of DM in galaxies, different models have been proposed, such as power-law profile, Navarro-Frenk-White (NFW) profile (Navarro et al. 1996; Navarro et al. 1997) and Hernquist profile (Hernquist 1990). These models explain the mass density of galactic DM well, while still leaving large uncertainty in galactic centers which are usually accompanied by massive black holes. In Gondolo & Silk (1999) (hereafter referred to as GS) it is found that DM would be accreted and redistributed in the presence of a black hole, forming a high-density spike that might be observable through gamma rays from annihilation. Moreover, fully relativistic spikes in the vicinity of Schwarzschild black holes (Sadeghian et al. 2013) and Kerr black holes (Ferrer et al. 2017) were investigated (hereafter referred to as SFW and FRW, respectively), confirming the presence of spike but with different profiles.

To probe the density profile of DM spike, GW might serve as a feasible new way. The inaugural discovery of GW (Abbott et al. 2016) has significantly invigorated study in black hole physics and the detection of GWs from super-massive black holes (ranging from $10^4 M_\odot$ to $10^9 M_\odot$). Concurrently, these topics form the cornerstone of upcoming space-based GW observatories like LISA (Amaro-Seoane et al. 2017; Baker et al. 2019), Taiji (Hu & Wu 2017; Ruan et al. 2020) and TianQin (Luo et al. 2016). The seminal work by Chandrasekhar (1943) on the general dynamical

friction established that the frictional force is proportional to the density of the surrounding environment, which has been utilized in recent discussions on using GWs to probe DM near black holes (Eda et al. 2013; Bertone et al. 2020; Kavanagh et al. 2020; Coogan et al. 2022; Cole et al. 2023; Zhang et al. 2024) and extended to wider context (Traykova et al. 2021a, 2023; Bamber et al. 2023; Boudon et al. 2022, 2023; Liang et al. 2023; Boey et al. 2024). As a compact object orbits around the central black hole, it is subjected to DF from the surrounding DM, which changes the orbital trajectory and furthermore affects the GWs emitted by such a binary (Macedo et al. 2013). Notable observational targets are intermediate-mass-ratio inspirals (IMRIs) and extreme-mass-ratio inspirals (EMRIs), the binaries consisting of a supermassive black hole and a compact object with a much smaller mass. It was demonstrated that DM minispikes could elevate the merger rate of IMRIs (Yue et al. 2019), potentially affecting the detectable event rate by LISA. Additionally, the impact of DM spikes on stellar orbits in the Galactic center has been explored (Shen et al. 2023), and in the future higher-resolution S-star observations will provide more accurate estimations of the parameters of the DM spikes. Although it was mentioned that galactic merging (Merritt et al. 2002) and stellar motion (Merritt 2004; Bertone & Merritt 2005) might kick out and disrupt the DM profiles in galaxies, in scenarios where massive black holes have avoided major mergers, DM minihalos can coexist nearby (Zhao & Silk 2005).

Considerable efforts had been devoted to the study of orbital dynamics and GW emission based on power-law profile or fitting adiabatic growth formula for the density of DM generating DF (Yue & Han 2018; Yue & Cao 2019; Hannuksela et al. 2020; Tang et al. 2021; Speeney et al. 2022). However, these discussions ignored the velocities of the DM particles. In fact, the effect of velocity distribution plays an important role because Chandrasekhar’s formula suggests that only particles below the orbital velocity of compact bodies are contributing DF. In this regard, Li et al. (2022) and Becker et al. (2022) discussed the effect of particle velocity distribution on orbital circularity or ellipticity, and showed that high-speed particles do not participate in gravity drag, which inevitably weakens DF. Besides, Karydas et al. (2024) introduced the circularizing effects of accretion of DM on secondary objects eccentricity evolution and the velocity distribution of DM was considered in numerical simulations (Kavanagh et al. 2024). However, relativistic effects near black holes were rarely considered, such as the relativistic density and velocity distribution after adiabatic growth. Because near the horizon of a black hole or when the binary is close to merge, we expect the system is generically relativistic and it would be more consistent to take such an effect into consideration.

In this paper, we calculate the velocity distributions of relativistic DM spikes formed by the adiabatic growth of Schwarzschild black holes from initial Hernquist dark halos or power-law dark halos. We employ the geodesic equations in the numerical calculations to account for the velocities of DM particles, and categorize them accordingly, leading to the identification of spikes formed by DM particles up to different maximum velocities. We also evaluate velocity distribution and fit with the Gauss distribution. Then, taking velocity into account and adding the relativistic DF formula, we illustrate with the GWs of EMRIs up to 3PN (post-Newtonian) eccentric gravitational radiation and demonstrate the phase shifts of waveforms in time domain.

This paper is structured as follows. In Section 2, we elaborate on how the adiabatic growth of the black hole modifies the original dark halo profile. This involves considering the conditions for black hole capture and evaluating the velocity distribution based on particle geodesic velocity. In Section 3, we shed light on the velocity distribution and the energy-momentum loss resulting from GW emission and DF from DM spikes. Then we calculate the GW signals by integrating the geodesic equations of the compact object to derive the orbital trajectories. Finally in Section 4 we show the numerical results, and summarize in Section 5.

2. DARK MATTER SPIKE

We first outline the relevant theoretical formalism and conventions (Sadeghian et al. 2013), including the relativistic dynamics and kinematics in the Schwarzschild metric. After obtaining the analytic formulas, we shall solve these equations numerically in later sections.

2.1. DM growth around Schwarzschild black hole

For a system of DM particles with given relativistic phase space distribution $f^{(4)}(x, p)$, the mass current four-vector can be expressed as

$$J^\mu(x) = \int f^{(4)}(x, p) u^\mu \sqrt{-g} d^4p, \quad (1)$$

where p is the four-momentum, $u^\mu = p^\mu/\mu$ is the four-velocity, μ is rest mass, g is the determinant of the metric, and d^4p is the four-momentum volume element. The distribution function $f^{(4)}(x, p)$ of DM is normalized, $\int f^{(4)}(x, p) \sqrt{-g} d^4p = 1$.

Using the relations $J^\mu = \rho u^\mu$ and $u_\mu u^\mu = -1$, we can obtain the density in a local free-falling frame $\rho = \sqrt{-J_\mu J^\mu}$. Therefore, the estimation of the components of J^μ is the main task. In general we can get the distribution function by Eddington formula (Eddington 1916) with a given density. However, it is not useful here because the density is unknown. In addition, the integral boundary of four-momentum volume element is undetermined, which results in the difficulty to integrate directly. Fortunately, we can overcome these by converting the integral element d^4p into the phase space of invariant constants of motion and leveraging the adiabatic invariance of the distribution function. Then using numerical integration we can obtain the components of J^μ .

The line element in Schwarzschild metric for a black hole of mass M (with the speed of light $c = 1$) can be written as

$$ds^2 = -(1 - \frac{2GM}{r})dt^2 + \frac{r}{r - 2GM}dr^2 + r^2 d\theta^2 + r^2 \sin^2 \theta d\phi^2. \quad (2)$$

Due to spherical symmetry, four constants of motion admitted by timelike geodesics are

$$\begin{aligned} \varepsilon &\equiv -u_t = -g_{tt}u^t, \quad \mu = \sqrt{-p_\mu p^\mu}, \\ L^2 &\equiv (g_{\theta\theta}u^\theta)^2 + \frac{L_z^2}{\sin^2 \theta} = (u_\theta)^2 + \frac{(u_\phi)^2}{\sin^2 \theta}, \\ L_z &\equiv u_\phi = g_{\phi\phi}u^\phi, \end{aligned} \quad (3)$$

where ε is the energy per unit mass, L_z is the angular momentum per unit mass, and L^2 is the the square of the conserved total angular momentum per unit mass. Then the integration element d^4p can be changed to the volume element of four constants of the motion $d\varepsilon dL^2 dL_z d\mu$.

Assuming all DM particles in the system have the same rest mass μ_0 , then the mass distribution is a δ function. Thus the distribution function can be simplified as $f^{(4)}(x, p) = \mu^{-3} f(\varepsilon, L^2, L_z) \delta(\mu - \mu_0)$. The element $d\mu$ is allowed to be integrated over. For later discussions, we just drop the subscript for simplicity. Considering the \pm signs of u^μ , we find that only the t components of J^μ would not vanish in Schwarzschild case. We set $\theta = \pi/2$ to simplify further calculation thanks to the spherical symmetry of Schwarzschild metric. Finally the nonzero component of the mass current four-vector is

$$J_t(r) = -\frac{2}{r^2} \iiint d\varepsilon dL^2 dL_z \frac{\varepsilon f(\varepsilon, L^2, L_z)}{\sqrt{V(r)} \sqrt{L^2 - L_z^2}}, \quad (4)$$

where

$$V(r) = \varepsilon^2 - (1 - \frac{2GM}{r})(1 + \frac{L^2}{r^2}), \quad (5)$$

and the density of DM spike is $\rho = \sqrt{-g^{tt}} |J_t|$.

We evaluate the phase space by the capture conditions of the black hole as in FRW (Ferrer et al. 2017). It is assumed that only DM particles in bound orbits contribute to the density of spike, which means that we should take out the orbits which plunge in the black hole. We apply three constraints: $\varepsilon_{max} = 1$, $V(r) \geq 0$ and $U(\theta) \geq 0$. Here

$$U(\theta) = L^2 - \frac{L_z^2}{\sin^2 \theta}. \quad (6)$$

The potential $V(r)$ has a minimal value at unstable orbit r_{unst} , which hints that $dV(r)/dr = 0$ and $d^2V(r)/dr^2 > 0$. Imposing the positivity of $U(\theta)$, integration region can be put in the parameter space of $(x, y, z) = [0, 1] \times [0, 1] \times [0, 1]$ as below,

$$\begin{aligned} \varepsilon(x) &= x + (1 - x)\varepsilon_{min}, \\ L^2(y) &= yL_{max}^2 + (1 - y)L_{crit}^2, \\ L_z(y, z) &= (2z - 1) |L(y)|. \end{aligned} \quad (7)$$

It allows the step size of the numerical integration to be fixed, thus facilitates our integration implementation. By setting $L_z = \pm\sqrt{L^2}$ and $\varepsilon = 1$ in $V(r)$, we obtain L_{max}^2 . For critical orbits, it requires that $\varepsilon = \varepsilon_{min}$ and $L^2 = L_{crit}^2$ at unstable orbit r_{unst} . Meanwhile, $V(r) = 0$ has a double root. These imply that we should solve a system of four polynomial equations of $(\varepsilon_{min}, L_{crit}^2, r_{unst}, L_z')$,

$$V(r) = 0, U(\theta) = 0, \frac{dV(r)}{dr}(r = r_{unst}) = 0, V(r_{unst}) = 0. \quad (8)$$

Now the integral boundary is fully determined.

We assume an initial spherically symmetric DM halo without a central black hole, which has a distribution function $f'(E', L'^2, L'_z)$ and gravitational potential $\Phi(r)$. Here E' is classical energy per particle mass. The adiabatic growth of the black hole in the halo keeps $f'(E', L'^2, L'_z) = f(\varepsilon, L^2, L_z)$. It means that the form of the distribution function is preserved.

Through the adiabatic growth, the integrals of motion of the system are invariant. The adiabatic invariants consist of three components for r, θ and ϕ . Since both the initial dark halo and the Schwarzschild spacetime are spherically symmetric, matching $I'_\theta = I_\theta$ and $I'_\phi = I_\phi$, we obtain $L'_z = L_z$ and $L' = L$. The focus of the calculation is then about radial integral of motion. The radial adiabatic invariant for a nonrelativistic DM particle is

$$I'_r(E', L') = \oint dr \sqrt{2E' - 2\Phi - \frac{L'^2}{r^2}}. \quad (9)$$

For the orbit of a DM particle in the Schwarzschild geometry,

$$I_r(\varepsilon, L^2, L_z) = \oint u_r dr = \oint dr \frac{\sqrt{V(r)}}{1 - 2GM/r}. \quad (10)$$

Considering the the form $1/r$ similar to the near center of NFW model, we use Hernquist profile to estimate the equation $I'_r = I_r$. Hernquist profile has the density function of

$$\rho_H = \frac{\rho_0}{(r/r_s)(1 + r/r_s)^3}, \quad (11)$$

with Newtonian gravitational potential

$$\Phi_H = -\frac{GM_{halo}}{r + r_s}, \quad (12)$$

where r_s and ρ_0 are scale factors. $M_{halo} = 2\pi\rho_0 r_s^3$ is the total mass of DM halo. For the Milky Way, we could take M_{halo} to be $10^{12}M_\odot$ and $r_s = 20\text{kpc}$. The distribution function of the profile was analytically derived by [Hernquist \(1990\)](#):

$$f_H(\tilde{\varepsilon}) = \frac{M_{halo}}{\sqrt{2}(2\pi)^3(GM_{halo}r_s)^{3/2}} \tilde{f}_H(\tilde{\varepsilon}), \quad (13)$$

where

$$\tilde{f}_H(\tilde{\varepsilon}) = \frac{\sqrt{\tilde{\varepsilon}}}{(1 - \tilde{\varepsilon})^2} \left[(1 - 2\tilde{\varepsilon})(8\tilde{\varepsilon}^2 - 2\tilde{\varepsilon} - 3) + \frac{3\sin^{-1}\sqrt{\tilde{\varepsilon}}}{\sqrt{\tilde{\varepsilon}(1 - \tilde{\varepsilon})}} \right]. \quad (14)$$

Here $\tilde{\varepsilon}$ is a new dimensionless relative energy. It is related to energy E' per unit particle mass or relativistic energy ε per unit particle mass by $\tilde{\varepsilon}' = -r_s E' / GM_{halo}$ in Newtonian case and $\tilde{\varepsilon} \equiv r_s(1 - \varepsilon) / GM_{halo}$ in relativistic case, respectively. Other dimensionless quantities are introduced below,

$$\tilde{M} \equiv \frac{M}{M_{halo}}, x \equiv \frac{r}{r_s}, \tilde{L} \equiv \frac{L}{\sqrt{GM_{halo}r_s}}, \tilde{L}_z \equiv \frac{L_z}{GM_{halo}r_s}, \tilde{\psi} \equiv -\frac{r_s}{GM_{halo}}\Phi = \frac{1}{1+x}. \quad (15)$$

Then we adopt the radial invariant for Hernquist profile and Schwarzschild geometry by substituting dimensionless relative energy $\tilde{\varepsilon}$ and Eq. (15) into Eq. (9) and Eq. (10):

$$\begin{aligned} I_r^H &= 2\sqrt{GM_{halo}r_s} \int_{x_-}^{x_+} dx \sqrt{-2\tilde{\varepsilon}' + \frac{2}{1+x} + \frac{\tilde{L}^2}{x^2}}, \\ I_r^S &= 2\sqrt{GM_{halo}r_s} \int_{x_-}^{x_+} dx \sqrt{-2\tilde{\varepsilon} + 2\frac{\tilde{M}}{x} - \frac{\tilde{L}}{x^2} + \frac{\tilde{\varepsilon}^2 GM_{halo}}{r_s} + \frac{2GM_{halo}}{r_s} \frac{\tilde{M}\tilde{L}^2}{x^3}}, \end{aligned} \quad (16)$$

where x_\pm are the two positive roots of function in the square root which represent the turning points of the orbit. For a set of (x, y, z) in phase space, equating Eq. (9) to Eq. (10) gives $\tilde{\varepsilon}$ and \tilde{L} . Because the radial invariant tends to be divergent as $\tilde{\varepsilon} \rightarrow 0$, we adopt the operation similar to SFW, and rewrite the integrals of radial invariants into the domain

$[0, 1]$, to ensure the stability of numerical integration. Hence, using the result that $f_H(\tilde{\epsilon}) = f(\varepsilon, L^2, L_z) = f(x, y, z)$, the integration of $J_t(r)$ could be evaluated at specific distance r .

Once the distribution function and adiabatic invariants are given, we can employ the above method to evaluate arbitrary DM spike densities near black holes. For instance, we consider a power-law initial dark halo $\rho_p(r) = \rho_0(r_s/r)^\gamma$, with $0 < \gamma < 2$. In terms of dark halo mass $M_{halo} = 4\pi\rho_0 r_s^3/(3 - \alpha)$ and dimensionless quantities, we rewrite the phase space distribution and radial adiabatic invariant [Gondolo & Silk \(1999\)](#),

$$\begin{aligned} f(\tilde{\epsilon}) &= \frac{\rho_0 r_s^{3/2} (2 - \gamma)^{3/2}}{(2\pi G M_{halo})^{3/2}} \frac{\Gamma(\beta)}{\Gamma(\beta - \frac{3}{2})} \left[-\frac{1}{(2 - \gamma)\tilde{\epsilon}} \right]^\beta, \\ I_r^p &= 2\sqrt{G M_{halo} r_s} \frac{B\left(\frac{1}{2-\gamma}, \frac{3}{2}\right)}{2 - \gamma} \left[-\frac{\tilde{L}}{\lambda} + \sqrt{\frac{2}{2 - \gamma}} [-(2 - \gamma)\tilde{\epsilon}]^{\frac{4-\gamma}{2(2-\gamma)}} \right], \end{aligned} \quad (17)$$

where $\beta = (6 - \gamma)/[2(2 - \gamma)]$ and $\lambda = [2/(4 - \gamma)]^{1/(2-\gamma)}[(2 - \gamma)/(4 - \gamma)]^{1/2}$. Thus, we can use the above expressions to calculate the spike that grows from a power-law dark halo.

2.2. Velocity distribution of DM Spike

Above we have described how to calculate the total density of DM spike around a Schwarzschild black hole. It would be more useful if we can also get the velocity distribution of DM particles, which is needed in the estimation of dynamical friction.

For given constants of motion (ε, L^2, L_z) , dividing the r , θ and ϕ components of the geodesics by the t component, we obtain the three velocity components in spherical coordinates,

$$v^r = \frac{u^r}{u^t}, v^\theta = \frac{u^\theta}{u^t}, v^\phi = \frac{u^\phi}{u^t}. \quad (18)$$

And the four velocity is written as $u^\mu = \gamma(1, v^j)$, where $v^j = u^j/u^t$ and $u^t = \gamma = (-g_{tt} - g_{ij}v^i v^j)^{-1/2}$. We obtain in Schwarzschild spacetime

$$\varepsilon^2 = -\frac{(-g_{tt})^2}{g_{tt} + v^2}, \quad (19)$$

where $v = \sqrt{g_{ij}v^i v^j}$. Then we can change the integration variable from ϵ to v in Eq. (4), and obtain

$$\frac{d\rho}{dv} = \frac{2v(-g_{tt})^{3/2}}{r^2(g_{tt} + v^2)^2} \iint dL^2 dL_z \frac{f(v, L^2, L_z)}{\sqrt{V(r)}\sqrt{L^2 - L_z^2}}. \quad (20)$$

We could presume that Eq. (20) is an isotropic velocity distribution which depends on r . Eq. (4) and Eq. (20) gives the spike density and the velocity distribution respectively, and they are closely correlated. In this paper we shall calculate the density first and then take the derivative to get the distribution function.

At each Monte Carlo sampling, the particle velocity can be calculated for a given set of sample (x, y, z) , which provides the access to construct the correlation between spike density and particle velocity. We limit the range of particle velocities with escape velocity $v_{max} = \sqrt{2GM/r}$. Apparently, v_{max} is a function of r . So the upper bounds on velocity are different at various distances. Therefore, we quantify the particle velocity by escape velocity $v_{max}(r)$ and define an unitized velocity v/v_{max} to transform the region of value into $[0, 1]$. Restriction could be imposed on the Monte Carlo integration process of mass current four-vector to count the DM particles at distance r that contribute to the density of spike and move slower than a certain velocity. We call the result velocity distribution of density $\rho(r, < v/v_{max})$ in this case. Naturally, we obtain $\rho = 0$ as $v/v_{max} = 0$ and $\rho_{max}(r)$ as $v/v_{max} = 1$. We assume that DM particles have the following velocity distribution representation in three-dimensions velocity phase space:

$$\rho(r, < \alpha = v/v_{max}) = \int_0^\alpha f'(r, \alpha) d^3\alpha, \quad (21)$$

here we replace v with α . By differentiating the density by quantified velocity $\alpha = v/v_{max}$, and redefine the isotropic velocity distribution function:

$$f(r, \alpha = v/v_{max}) = \frac{1}{\rho(r, 1)} \frac{d\rho(r, \alpha)}{d\alpha} = \frac{4\pi\alpha^2 f'(r, \alpha)}{\rho(r, 1)}. \quad (22)$$

Given the distance r and velocity v to infer the value of α , $\rho(r, \alpha)$ represents the density constructed by the DM particles whose velocity below the v . We will present the results under various parameter conditions to intuitively reflect the accumulation of DM particles around black hole in Section 4. In the following Section 3, we elucidate the DF effects of DM density with velocity distribution on the orbiting objects in EMRIs and investigate the impact on the GW from EMRIs.

3. EFFECTS ON GRAVITATIONAL WAVES FROM EMRIS

Now we are in a position to consider the effects on EMRI from a DM spike. We shall include the DF of DM as well as 3PN gravitational radiation reaction (Sago & Fujita 2015) to obtain the orbital energy loss and the evolution of the constants of motion. Introducing the evolving constants of motion, we construct numerical kludge waveform (Babak et al. 2007) to compute the orbital trajectory of orbiting body. Then we could calculate the GW waveform with or without DF.

3.1. Gravitational radiation and Dynamical Friction

In the Schwarzschild spacetime, the orbit stays in a plane and consequently we can obtain the orbital trajectory $(r(t), \phi(t))$ of test body by integrating the geodesic equations,

$$\begin{aligned}\frac{dt}{d\tau} &= \frac{E}{1 - 2GM/r}, \\ \frac{dr}{d\tau} &= \pm \sqrt{E^2 - \left(1 - \frac{2GM}{r}\right) \left(1 + \frac{L^2}{r^2}\right)}, \\ \frac{d\phi}{d\tau} &= \frac{L_z}{r^2}.\end{aligned}\tag{23}$$

Numerical integration can be optimized by defining

$$r = \frac{p}{1 + e \cos \psi}.\tag{24}$$

Here p is semi-latus rectum and e is orbital eccentricity. Then we work with ψ and ϕ , instead of r and ϕ . We combine Eq. (23) and Eq. (24), then obtain the equation for ψ ,

$$\frac{d\psi}{dt} = \frac{\sqrt{(1 - E^2)p(p - er_{in}(1 + e \cos \psi))}}{E\sqrt{1 - e^2}r^3/(r - 2GM)},\tag{25}$$

where r_{in} is one of the zero points of the equation $dr/d\tau$, which is located inside the horizon. The other two zero points are the turning points of the orbit, expressed by $r_a = p/(1 - e)$ and $r_p = p/(1 + e)$. The evolution equation Eq. (25) corresponds to the Schwarzschild limit of the result of Babak et al. (2007).

Taking GW radiation reaction into account, the orbital constants dissipate over time,

$$\left(\frac{dE}{dt}\right)_{\text{GW}} = g_E(m, M, p, e), \quad \left(\frac{dL_z}{dt}\right)_{\text{GW}} = g_{L_z}(m, M, p, e).\tag{26}$$

We consider the 3PN back-reaction of the orbital constants (Sago & Fujita 2015). In this way, gravitational radiation is introduced into geodesic motion. Moreover, orbiting objects are dragged by the gravity of the surrounding matter, causing energy loss. Since the velocities of DM particles near black holes are around $\mathcal{O}(10^{-1})$ of the speed of light c , we consider relativistic DF force (Barausse 2007; Traykova et al. 2021b) described by

$$\left(\frac{dE}{dt}\right)_{\text{DF}} = F_{\text{DF}} \cdot v = -\frac{4\pi\rho(r, < v)G^2m^2\gamma^2[1 + (v/c)^2]^2}{v} \ln \Lambda,\tag{27}$$

where $\gamma = 1/\sqrt{1 - (v/c)^2}$ is the Lorentz factor, and $\ln \Lambda$ is the Coulomb logarithm adopted as 10. In this framework, the energy loss from gravitational drag is contributed by the DM particles whose velocities are below the orbiting relativistic compact object. Similarly, the angular momentum loss rate is

$$\left(\frac{dL_z}{dt}\right)_{\text{DF}} = r \cdot F_{\text{DF}} \frac{r\dot{\psi}}{v} = -\frac{4\pi\rho(r, < v)G^2m^2r^2\dot{\psi}\gamma^2[1 + (v/c)^2]^2}{v^2} \ln \Lambda.\tag{28}$$

Put the above together, we have the evolution equations for energy and angular momentum,

$$\frac{dE}{dt} = \left(\frac{dE}{dt}\right)_{\text{GW}} + \left(\frac{dE}{dt}\right)_{\text{DF}}, \quad \frac{dL_z}{dt} = \left(\frac{dL_z}{dt}\right)_{\text{GW}} + \left(\frac{dL_z}{dt}\right)_{\text{DF}}. \quad (29)$$

Combining with the geodesic equation and solving numerically, we obtain the trajectory of the orbiting object, which is used to calculate the corresponding gravitational waveform.

3.2. Gravitational Wave

Once we have solved the equations of motion for the orbit, we proceed to calculate the corresponding gravitational waves. Using quadrupole-octupole formula (Press 1977), we have the wave field

$$h_{jk}(t, \vec{x}) = \frac{2G}{c^4} \frac{1}{d} [\ddot{I}_{jk} - 2n_i \ddot{S}_{ijk} + n_i \ddot{M}_{ijk}]|_{t'=t-\frac{d}{c}}, \quad (30)$$

where I_{jk} is the mass quadrupole moment, S_{ijk} is the current quadrupole moment, M_{ijk} is the mass octupole moment, an overdot denotes a time-derivative, d is the distance from the source to detector, and n_i are the components of direction vector $\hat{\mathbf{n}} = \mathbf{d}/d = (\sin \theta_D \cos \phi_D, \sin \theta_D \sin \phi_D, \cos \phi_D)$, specified by the azimuth ϕ_D and latitude θ_D of the source in the sky. In the extreme-mass-ratio limit for point mass m (the mass ratio of binary is $m/M \ll 1$), the multipole moments are

$$\begin{aligned} I_{jk} &= m x_j x_k, \\ S_{ijk} &= m v_i x_j x_k, \\ M_{ijk} &= m x_i x_j x_k. \end{aligned} \quad (31)$$

Here $x_{i,j,k}$ correspond to the components of the position in Cartesian coordinates (x, y, z) and $v_i = dx_i/dt$. Here and hereafter, (m, M, d) of the source are referred as the redshifted masses and luminosity distance.

Projecting the waveform in the transverse-traceless (TT) gauge, we have the plus (+) and the cross (×) polarizations of waveform, h_+ and h_\times ,

$$h_{jk}^{TT} = \begin{pmatrix} 0 & 0 & 0 \\ 0 & h_+ & h_\times \\ 0 & h_\times & -h_+ \end{pmatrix}. \quad (32)$$

When taking into account the responses of space-based GW detectors like LISA and Taiji, it is convenient to consider the strain $h_{I,II}$, which are linear combinations of h_+ and h_\times ,

$$h_I = \frac{\sqrt{3}}{2} (F_I^+ h_+ + F_I^\times h_\times), \quad h_{II} = \frac{\sqrt{3}}{2} (F_{II}^+ h_+ + F_{II}^\times h_\times), \quad (33)$$

where $F^{+, \times}$ are antenna pattern functions (Apostolatos et al. 1994). The polarization angle of the source ψ_D in $F^{+, \times}$ is given by

$$\psi_D = \arctan \left(\frac{\hat{\mathbf{L}} \cdot \hat{\mathbf{z}} - (\hat{\mathbf{L}} \cdot \hat{\mathbf{n}})(\hat{\mathbf{z}} \cdot \hat{\mathbf{n}})}{\hat{\mathbf{n}} \cdot (\hat{\mathbf{L}} \times \hat{\mathbf{z}})} \right). \quad (34)$$

ψ_D depends on the unit vector $\hat{\mathbf{L}}$ of orbital angular momentum \mathbf{L} and the basis vector $\hat{\mathbf{z}}$ of the z-axis in detector-based coordinate system. For a orbit in equatorial plane, angular momentum \mathbf{L} is conserved. Thus the unit vector $\hat{\mathbf{L}}$ is a constant vector and ψ is constant. For illustration, we set $\psi_D = \pi/2$ ($\hat{\mathbf{L}} = \hat{\mathbf{z}}$) and $(\theta_D, \phi_D) = (\pi/2, 0)$ in later calculations. For the strain $h(t) = h_I + i h_{II}$ in time domain, we only show h_I because h_I and h_{II} have similar features.

4. RESULTS AND DISCUSSIONS

Now we demonstrate the density profiles of DM spikes growing from initial different halos around black holes of different sizes. We consider three cases for comparison. The physical parameters for each case are listed in Table. 1. Specifically, we consider a Hernquist dark halo around the black hole at the center of the Milky Way galaxy, a Hernquist

Table 1. Physical parameters of three cases

Case	Central black hole mass	Initial halo	Halo parameters	Index	Fitting parameters
	(M)	(Type)	(M_{halo}, r_s)	(γ)	(κ, η, ω)
C1	$4.6 \times 10^6 M_\odot$	Hernquist	($10^{12} M_\odot, 20$ kpc)	-	(5.33×10^{20} GeV/cm ³ , 1.99, 2.07)
C2	$10^4 M_\odot$	Hernquist	($4.5 \times 10^8 M_\odot, 1.85$ kpc)	-	(6.15×10^{24} GeV/cm ³ , 2.03, 2.11)
C3	$10^4 M_\odot$	Power law	($7.3 \times 10^8 M_\odot, 1.85$ kpc)	7/4	(5.83×10^{26} GeV/cm ³ , 2.04, 2.16)

NOTE—The initial parameters of the three cases we considered. We fit the profiles with Eq. (35), and present the best fitted parameters in the last column.

dark halo around a black hole with the mass $M = 10^4 M_\odot$ that corresponds to the case with a dwarf galaxy, and a power-law dark halo around a black hole with the mass $M = 10^4 M_\odot$.

Note that the DM halo mass M_{halo} and the scale r_s are correlated. For the case with black hole mass $M = 10^4 M_\odot$, we follow the approach of Nishikawa et al. (2019) and Hannuksela et al. (2020) to relate the halo parameters ρ_0 and r_s to central black hole mass M by mass-velocity-dispersion relation. Thus we can estimate the density of the DM spike around a black hole. For example, for $M = 10^4 M_\odot$, we obtain the halo scale factor $r_s = 1.85$ kpc and halo mass $M_{halo} \approx 4.5 \times 10^8 M_\odot$. The halo mass for Hernquist profile is determined by $M_{halo} = 2\pi\rho_0 r_s^3$, while halo with power-law profile $M_{halo} \approx 7.3 \times 10^8 M_\odot$ with scale $r_s = 1.85$ kpc. Here the power-law index is $\gamma = 7/4$.

In Figs. (1-3) we show the various density distributions over DM particles' velocities and/or positions from center for three cases. In each figure, the four plots correspond to density function over velocity at different fixed positions, density function over position with upper bounds on the velocity, velocity dispersion at different positions and two-dimensional density distribution over position and velocity, respectively. Besides the overall factor, the common features displayed in all three cases suggest the scale invariance of density distribution. Therefore, we shall elaborate the first case Fig. 1.

In plot (a), we show how the density changes as we put an upper bound on the DM's velocity at three locations, $r = 10GM, 20GM$ and $30GM$. It is seen that, as the velocity approaches v_{max} , the density reaches its maximum. It also indicates that at location closer to the black hole DM particles are more focused on larger velocities. This can be more easily understood from the velocity distributions in plot (c) which exhibits that both central values and widths of the velocity distributions are different at three locations. In plot (b), we demonstrate the density function over distance, only summing particles up to some velocities, v/v_{max} . These curves show that DM density increases as approaching black holes but goes to zero at $r = 4GM$ as no stable orbit exists $r < 4GM$, and the maximal density is around $r \simeq 8GM$. Plot (d) is a two-dimensional density distribution over position and the velocity of DM up to some value, which is useful in the evaluation of DF of DM spike.

Comparing Fig. 1 with Fig. 2, we find that the spike in the vicinity of a black hole with mass of $10^4 M_\odot$ is about three orders of magnitude higher than galactic central black hole at the same normalized distance $\bar{r} = r/GM$. The difference in Fig. 2 and Fig. 3 shows that the high densities are closely related to the initial DM halo profile. The power-law halo could generate a spike whose density is about two orders of magnitude higher than that from Hernquist halo, although both give similar mass for the galactic dark halo.

For potential use, we also fit the density total profiles below the maximum velocity $\alpha = v/v_{max} = 1$ to this form,

$$\rho(r, \alpha = 1) = \frac{\kappa}{(r/GM)^\omega} \left(1 - \frac{4GM}{r}\right)^\eta. \quad (35)$$

This corresponds to the black curve in plot (b). Here κ reflects the overall magnitude of density, ω represents the power-law change with distance, and η controls the size of the spike approaching to black hole. The profile vanishes as $r \leq 4GM$ due to the nonexistence of stable orbits of DM particles. The best fitted values of κ, ω and η are listed in the last column in Tab. 1. We can see in all cases $\eta \simeq 2$ and $\omega \simeq 2$.

Intrigued by the shape of velocity distribution in plot (c) in each figure, we fit it with Gaussian distribution,

$$f_r(v) = \frac{1}{\sqrt{2\pi}\sigma(r)} \exp\left(-\frac{(v - \bar{v}(r))^2}{2\sigma^2(r)}\right), \quad (36)$$

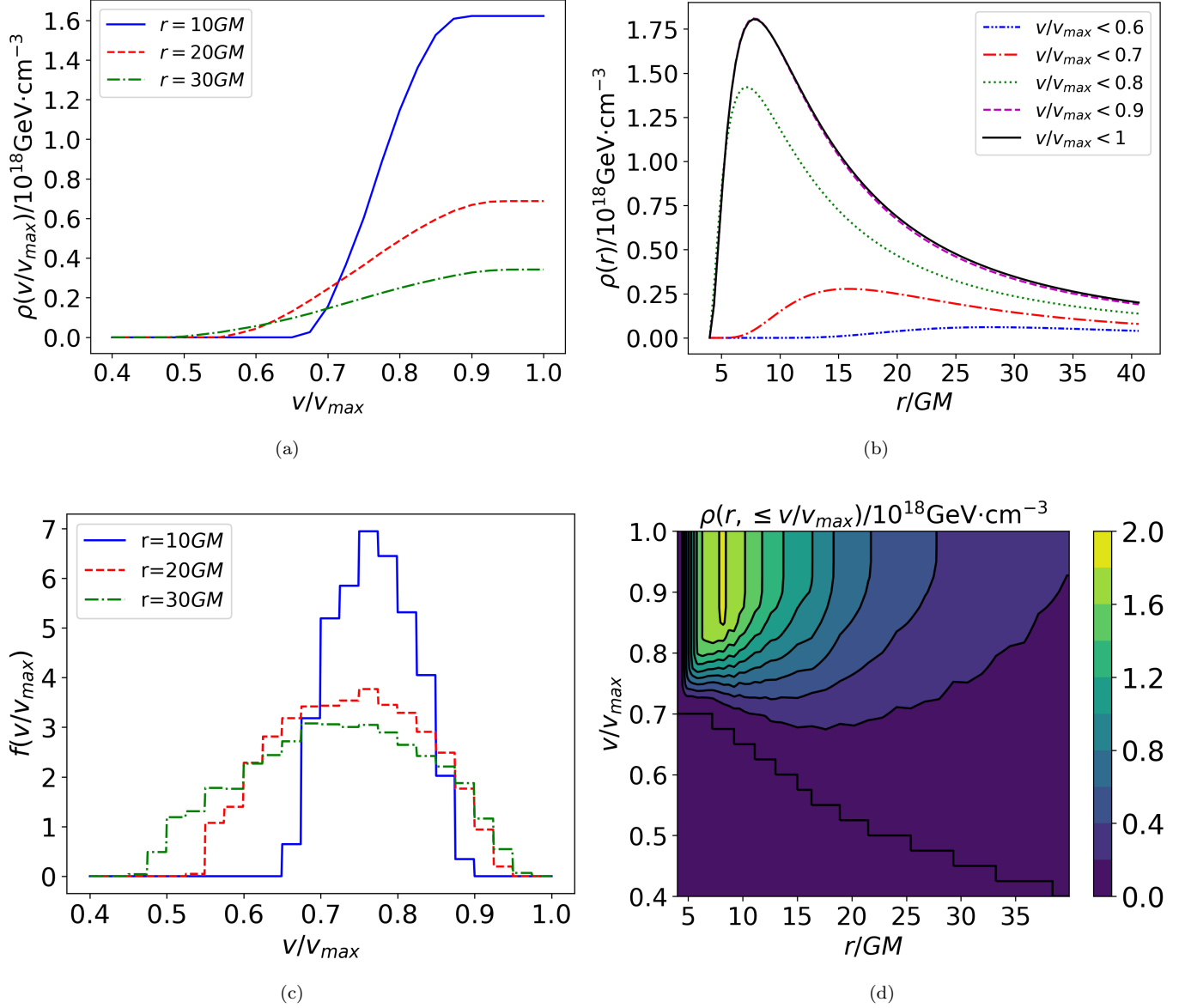


Figure 1. DM distribution around the black hole in Milky Way. Dark halo parameters (M_{halo}, r_s) are ($10^{12}M_{\odot}, 20\text{kpc}$). (a) The density-velocity relation $\rho(v/v_{\max})$ of DM at specific distances. (b) The density-distance relation $\rho(r)$ of DM below various velocities. (c) The DM distribution $f(v/v_{\max})$ of velocity at specific distances. (d) DM density $\rho(r, \leq v/v_{\max})$ in the $r - v/v_{\max}$ plane.

where $f_r(v)$ denotes the velocity distribution of DM particles at distance r , $\bar{v}(r)$ is the mean value of velocity at r , and variance $\sigma(r)$ shows the scale of velocity dispersion. We show the fitting results of Galactic Center black hole in Fig. 4. Plot (a) shows the numerically calculated points (original) and the fitting curve at several distances. We find that the particle velocity approaches a single value 0.5 when $r \rightarrow 4GM$. This is because that the closest bound circular orbit is uniquely determined at $r = 4GM$. The constants of motion (ε, L) in phase space are $(1, 4GM)$ (Sadeghian et al. 2013). Substituting it into geodesic equations we can derive that the particle at $r = 4GM$ has a circular motion with a velocity $v = 0.5$ (Hobson et al. 2006). The variations of \bar{v} and σ over distance r are demonstrated in plot (b) and (c) in Fig. 4, respectively. From the above analysis, we naturally set $\bar{v} = 0.5$ and $\sigma = 0$ at $r = 4GM$. Using such a distribution, we can simplify the calculation of DM spike density with velocity distribution close to Schwarzschild

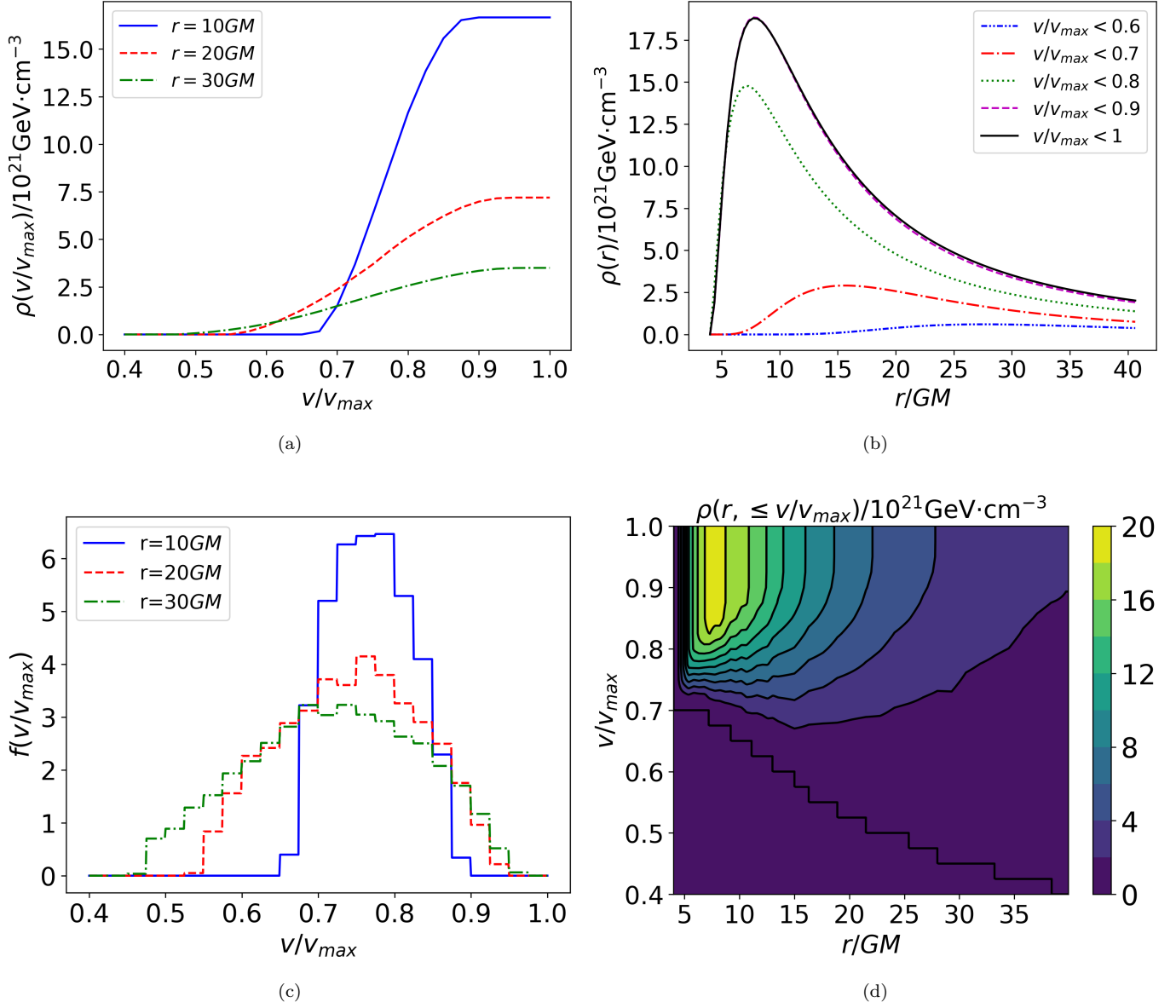


Figure 2. DM distribution around a black hole with mass $M = 10^4 M_\odot$ with an initial Hernquist profile. Dark halo parameters (M_{halo}, r_s) are $(4.5 \times 10^8 M_\odot, 1.85 \text{ kpc})$. (a) The density-velocity relation $\rho(v/v_{\text{max}})$ of DM at specific distances. (b) The density-distance relation $\rho(r)$ of DM below various velocities. (c) The DM distribution $f(v/v_{\text{max}})$ of velocity at specific distances. (d) DM density $\rho(r, \leq v/v_{\text{max}})$ in the $r - v/v_{\text{max}}$ plane.

black hole by

$$\rho(r, < v) = \rho(r, < 0.5) \int_0^v f_r(v) d^3 v. \quad (37)$$

Finally we are in a position to investigate the effects of DF from DM spikes on GWs. We illustrate with two typical EMRI systems with physical parameters $(m, M, e_0, p_0, d) = (10 M_\odot, 4.6 \times 10^6 M_\odot, 0.2, 8.5 \text{ GM}, 1 \text{ Gpc})$ and $(10 M_\odot, 10^4 M_\odot, 0.3, 30 \text{ GM}, 0.1 \text{ Gpc})$, respectively. We show the time-domain waveforms of h_I in Fig. 5 for three cases. The solid red lines (dotted green) represent GW waveform with (without) DF. The signals terminate when the orbiting compact objects nearly plunge (the instantaneous orbits become unstable). The duration is about 8 years in the upper panel of Fig. 5, and about one week in the other two cases.

We can observe in Fig. 5 that there is visible difference between GW waveforms with/without DF of DM spike in each case. The difference accumulates with time and in all three cases become sizable at plunge, which has been shown

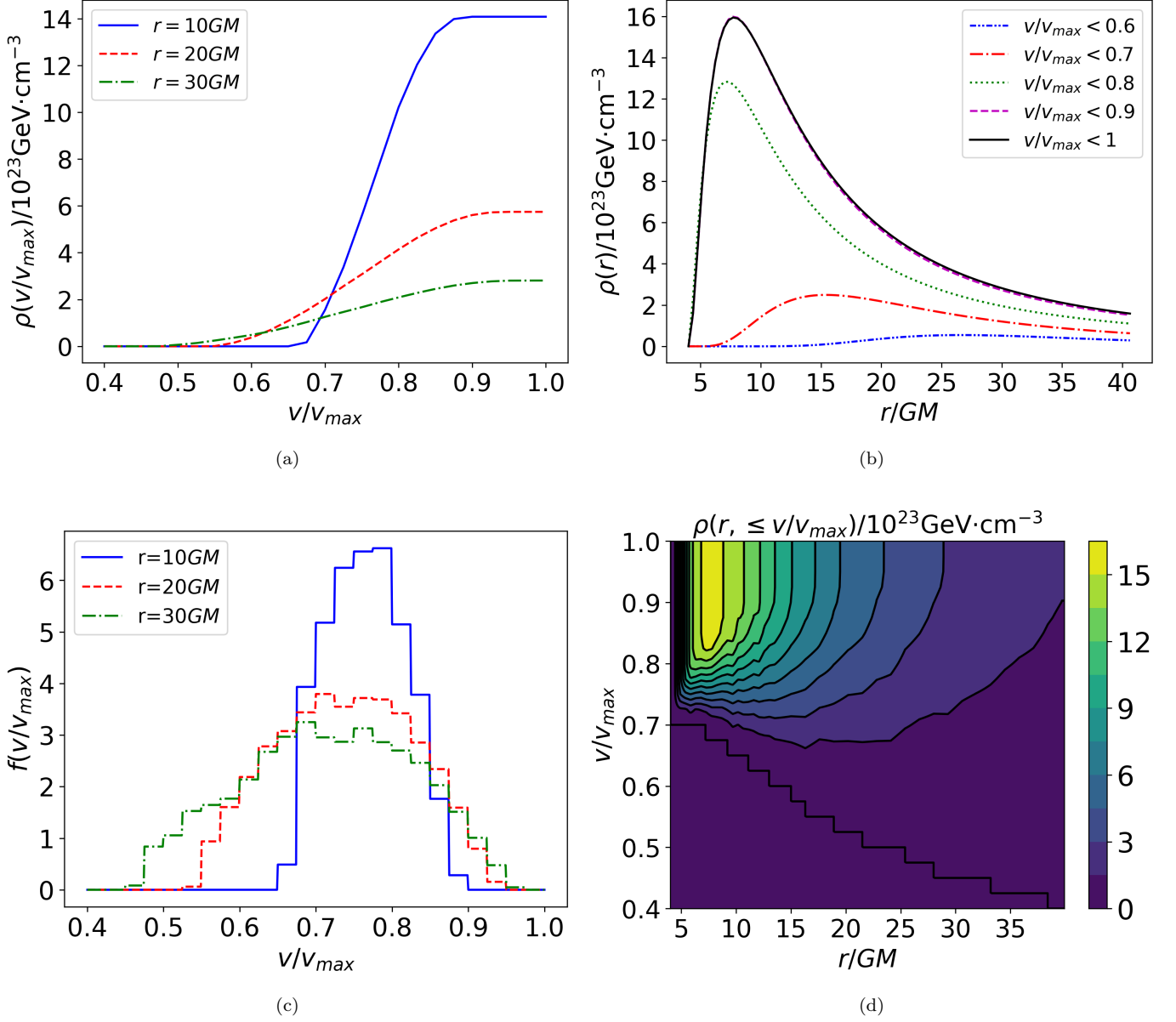


Figure 3. DM distribution around a center black hole with mass $M = 10^4 M_\odot$ with an initial power-law profile. Dark halo parameters ($M_{\text{halo}}, r_s, \gamma$) are $(7.3 \times 10^8 M_\odot, 1.85 \text{kpc}, 7/4)$. (a) The density-velocity relation $\rho(v/v_{\max})$ of DM at specific distances. (b) The density-distance relation $\rho(r)$ of DM below various velocities. (c) The DM distribution $f(v/v_{\max})$ of velocity at specific distances. (d) DM density $\rho(r, \leq v/v_{\max})$ in the $r - v/v_{\max}$ plane.

in the three small plots in each panel. We can also see that the effects of DF are stronger for smaller black holes. This can be easily understood as the DM density is larger near smaller black holes, as discussed above. Note that generally how larger the difference is also depends on the physical parameters of EMRIs. Here we just elucidate with several examples. For more quantitative parameter estimation, more dedicated analysis would be needed, which is beyond the scope here.

5. SUMMARY

We have evaluated the velocity and density distributions of DM particles in a spike around a Schwarzschild black hole in the relativistic case. By correlating the dark halo parameters with the mass of the central black hole, we have calculated the density of a DM spike from adiabatic growth of a black hole within a specific initial dark halo, such as

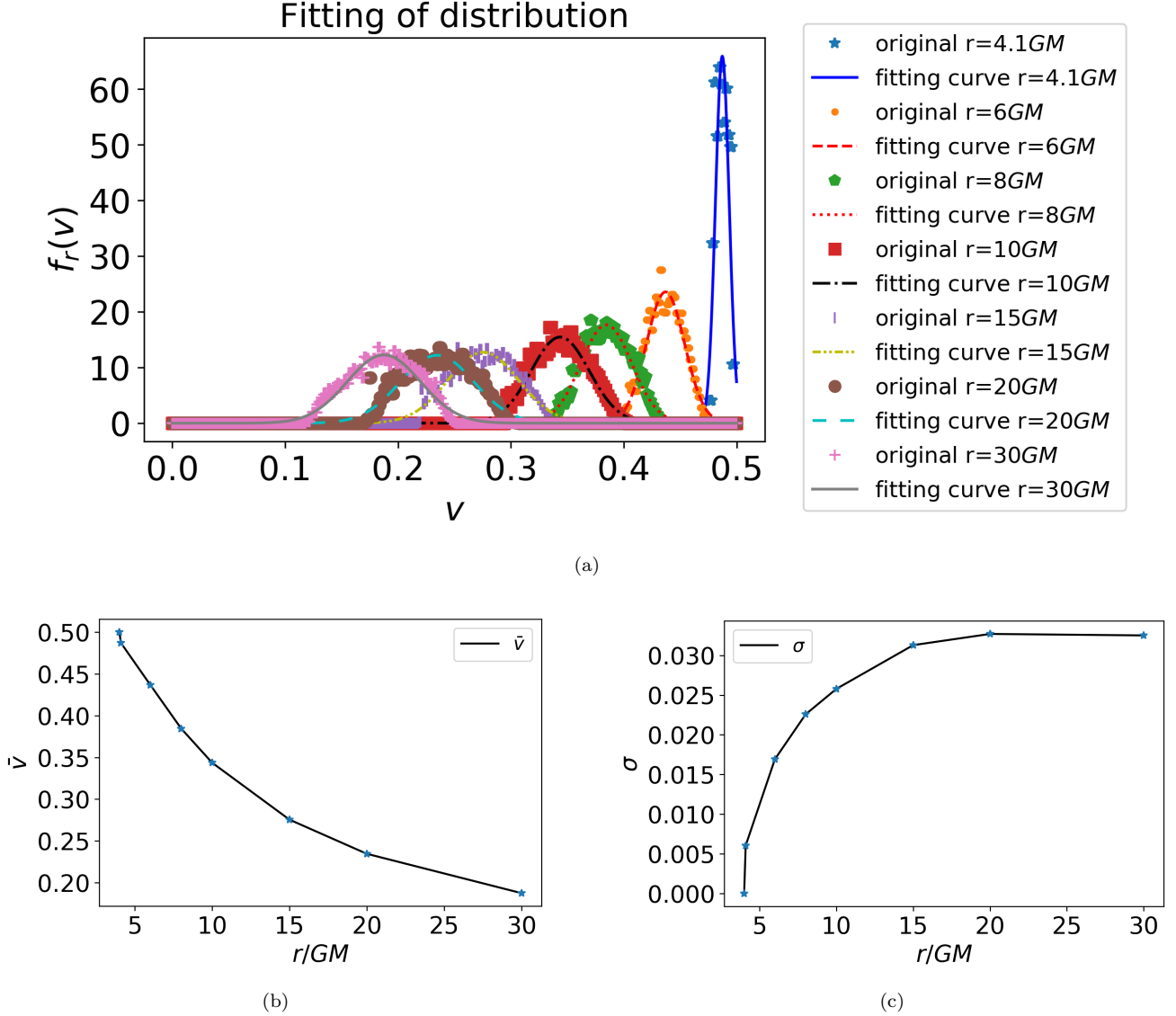


Figure 4. Fitting results from DM distribution around Galactic Center black hole. (a) Adapted distribution $f_r(v)$ at various distances with original scattering points. (b) The expected value \bar{v} varies with r . (c) The variance σ varies with r .

Hernquist profile and power-law profile. We have found that the density profile of the DM spike is scale invariant in its shape, but larger in magnitude at the same normalized distance $\bar{r} = r/GM$ for smaller central black hole within the same initial dark halo. In Hernquist dark halo, the DM spike surrounding a black hole with mass of $10^4 M_\odot$ is three orders of magnitude denser than that around the supermassive black hole in Milky Way. Moreover, the densities of spikes for different initial conditions could vary greatly. Near the black hole with mass of $10^4 M_\odot$, the spike that grows from a power-law halo is about two orders of magnitude higher than that from Hernquist halo.

We have also visualized the velocities of DM particles in the spike and fitted the spectrum with Gaussian distribution. This would simplify the subsequent DF calculation, where relativistic effect is taken into account. The result shows that the velocities of DM particles closer to the black hole tend to be narrowly distributed, while the velocities of particles far away scatter more widely.

Finally we have investigated the GW waveform of a stellar-mass compact object orbiting a massive black hole (EMRI) within a DM spike along general elliptical orbit. Those DM particles moving slower than the orbiting objects generate gravitational drag that can change the evolution of the object. In our results, such an effect, or DF of the

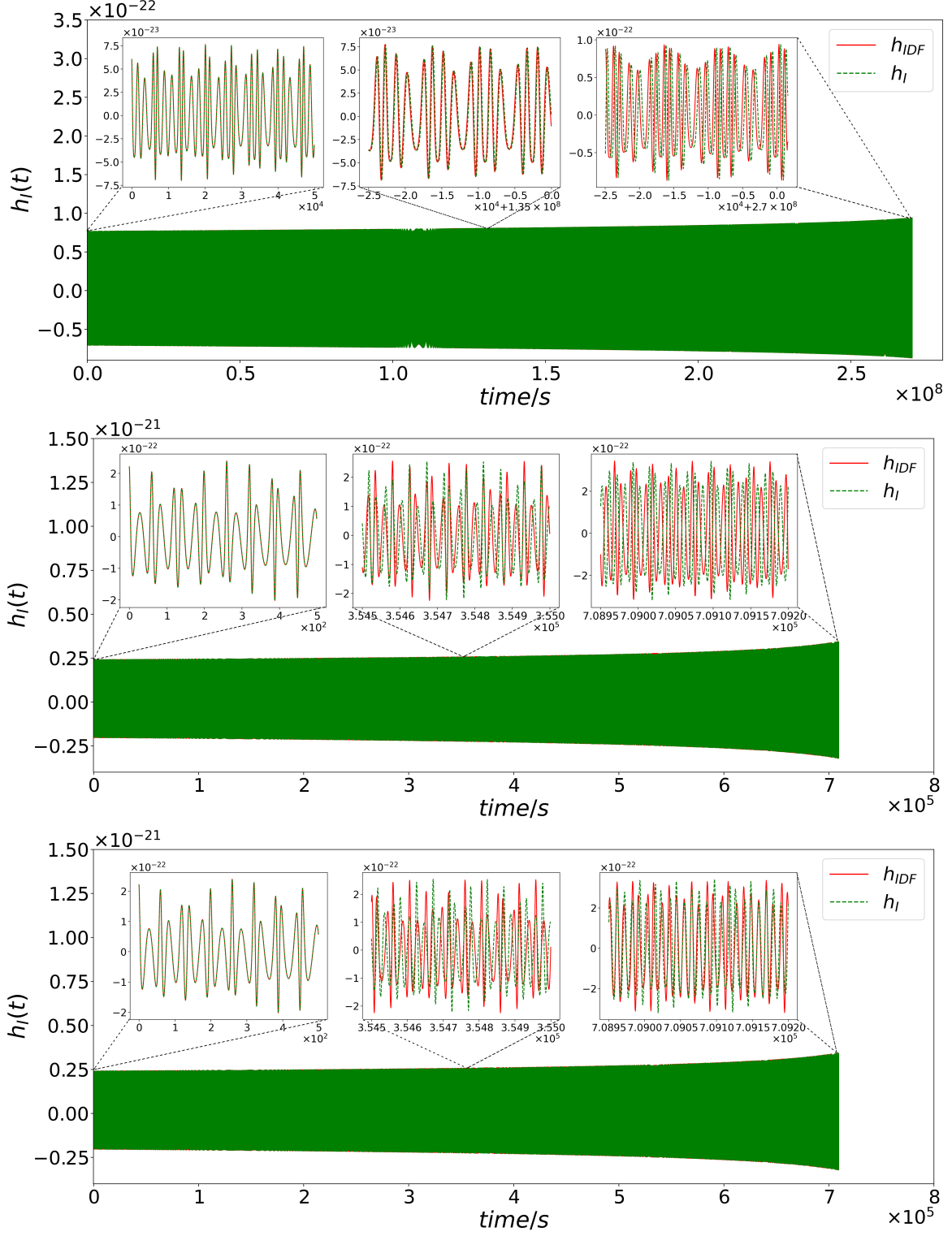


Figure 5. (Upper) GW waveform h_I of EMRI with $(m, M, e_0, p_0, d) = (10M_\odot, 4.6 \times 10^6 M_\odot, 0.2, 8.5GM, 1\text{Gpc})$ in a spike which grows from Hernquist initial dark halo with $(M_{\text{halo}}, r_s) = (10^{12}M_\odot, 20 \text{ kpc})$. (Middle) Waveform h_I of EMRI with $(m, M, e_0, p_0, d) = (10M_\odot, 10^4 M_\odot, 0.3, 30GM, 0.1 \text{ Gpc})$ in a spike which grows from Hernquist dark halo with $(M_{\text{halo}}, r_s) = (4.5 \times 10^8 M_\odot, 1.85 \text{ kpc})$. (Lower) Waveform h_I of EMRI with $(m, M, e_0, p_0, d) = (10M_\odot, 10^4 M_\odot, 0.3, 30GM, 0.1 \text{ Gpc})$ in a spike which grows from power-law dark halo with $(M_{\text{halo}}, r_s, \gamma) = (7.3 \times 10^8 M_\odot, 1.85 \text{ kpc}, 7/4)$. The solid red lines (dotted green) represent GW waveform with (without) DF.

spikes causes visible phase change in the waveform of GWs emitted from an EMRI, which is a potential source for future GW detectors in space, such as LISA and Taiji.

¹ This work is supported by the National Key Research and Development Program of China (Grant
² No.2021YFC2201901), the National Natural Science Foundation of China (Grant No.12147103) and the Fundamental
³ Research Funds for the Central Universities. We acknowledge the use of NumPy [Harris \(2020\)](#), SciPy [Virtanen \(2020\)](#),
⁴ and Matplotlib [Hunter \(2007\)](#) for numerical calculations and data visualization.

REFERENCES

- Abbott, B. P., Abbott, R., Abbott, T. D., et al. 2016, *Phys. Rev. Lett.*, 116, 061102, doi: [10.1103/PhysRevLett.116.061102](#)
- Amaro-Seoane, P., Audley, H., Babak, S., et al. 2017, *Laser Interferometer Space Antenna*.
<https://arxiv.org/abs/1702.00786>
- Apostolatos, T. A., Cutler, C., Sussman, G. J., & Thorne, K. S. 1994, *Phys. Rev. D*, 49, 6274, doi: [10.1103/PhysRevD.49.6274](#)
- Babak, S., Fang, H., Gair, J. R., Glampedakis, K., & Hughes, S. A. 2007, *Phys. Rev. D*, 75, 024005, doi: [10.1103/PhysRevD.75.024005](#)
- Baker, J., Bellovary, J., Bender, P. L., et al. 2019, *The Laser Interferometer Space Antenna: Unveiling the Millihertz Gravitational Wave Sky*.
<https://arxiv.org/abs/1907.06482>
- Bamber, J., Aurrekoetxea, J. C., Clough, K., & Ferreira, P. G. 2023, *Phys. Rev. D*, 107, 024035, doi: [10.1103/PhysRevD.107.024035](#)
- Barausse, E. 2007, *Monthly Notices of the Royal Astronomical Society*, 382, 826, doi: [10.1111/j.1365-2966.2007.12408.x](#)
- Becker, N., Sagunski, L., Prinz, L., & Rastgoo, S. 2022, *Phys. Rev. D*, 105, 063029, doi: [10.1103/PhysRevD.105.063029](#)
- Bertone, G., Hooper, D., & Silk, J. 2005, *Physics Reports*, 405, 279, doi: <https://doi.org/10.1016/j.physrep.2004.08.031>
- Bertone, G., & Merritt, D. 2005, *Phys. Rev. D*, 72, 103502, doi: [10.1103/PhysRevD.72.103502](#)
- Bertone, G., Croon, D., Amin, M. A., et al. 2020, *SciPost Phys. Core*, 3, 007, doi: [10.21468/SciPostPhysCore.3.2.007](#)
- Boey, R., Wang, Y., Kendall, E., & Easter, R. 2024, <https://arxiv.org/abs/2403.09038>
- Boudon, A., Brax, P., & Valageas, P. 2022, *Phys. Rev. D*, 106, 043507, doi: [10.1103/PhysRevD.106.043507](#)
- . 2023, *Phys. Rev. D*, 108, 103517, doi: [10.1103/PhysRevD.108.103517](#)
- Chandrasekhar, S. 1943, *ApJ*, 97, 255, doi: [10.1086/144517](#)
- Cole, P., Bertone, G., Coogan, A., et al. 2023, *Nature Astronomy*, 1, doi: [10.1038/s41550-023-01990-2](#)
- Coogan, A., Bertone, G., Gaggero, D., Kavanagh, B. J., & Nichols, D. A. 2022, *Phys. Rev. D*, 105, 043009, doi: [10.1103/PhysRevD.105.043009](#)
- Eda, K., Itoh, Y., Kuroyanagi, S., & Silk, J. 2013, *Phys. Rev. Lett.*, 110, 221101, doi: [10.1103/PhysRevLett.110.221101](#)
- Eddington, A. S. 1916, *MNRAS*, 76, 572, doi: [10.1093/mnras/76.7.572](#)
- Ferrer, F., Medeiros da Rosa, A., & Will, C. M. 2017, *Phys. Rev. D*, 96, 083014, doi: [10.1103/PhysRevD.96.083014](#)
- Gondolo, P., & Silk, J. 1999, *Phys. Rev. Lett.*, 83, 1719, doi: [10.1103/PhysRevLett.83.1719](#)
- Hannuksela, O. A., Ng, K. C. Y., & Li, T. G. F. 2020, *Phys. Rev. D*, 102, 103022, doi: [10.1103/PhysRevD.102.103022](#)
- Harris, C. R. e. a. 2020, *Nature*, 585, 357–362, doi: [10.1038/s41586-020-2649-2](#)
- Hernquist, L. 1990, *ApJ*, 356, 359, doi: [10.1086/168845](#)
- Hobson, M. P., Efstathiou, G. P., & Lasenby, A. N. 2006, *General Relativity: An Introduction for Physicists* (Cambridge University Press), doi: [10.1017/CBO9780511790904](#)
- Hu, W.-R., & Wu, Y.-L. 2017, *National Science Review*, 4, 685, doi: [10.1093/nsr/nwx116](#)
- Hunter, J. D. 2007, *Computing in Science & Engineering*, 9, 90, doi: [10.1109/MCSE.2007.55](#)
- IBARRA, A., TRAN, D., & WENIGER, C. 2013, *International Journal of Modern Physics A*, 28, 1330040, doi: [10.1142/S0217751X13300408](#)
- Karydas, T. K., Kavanagh, B. J., & Bertone, G. 2024, *Sharpening the dark matter signature in gravitational waveforms I: Accretion and eccentricity evolution*.
<https://arxiv.org/abs/2402.13053>
- Kavanagh, B. J., Karydas, T. K., Bertone, G., Cintio, P. D., & Pasquato, M. 2024, *Sharpening the dark matter signature in gravitational waveforms II: Numerical simulations with the NbodyIMRI code*.
<https://arxiv.org/abs/2402.13762>

- Kavanagh, B. J., Nichols, D. A., Bertone, G., & Gaggero, D. 2020, *Phys. Rev. D*, 102, 083006, doi: [10.1103/PhysRevD.102.083006](https://doi.org/10.1103/PhysRevD.102.083006)
- Li, G.-L., Tang, Y., & Wu, Y.-L. 2022, *Science China Physics, Mechanics, and Astronomy*, 65, 100412, doi: [10.1007/s11433-022-1930-9](https://doi.org/10.1007/s11433-022-1930-9)
- Liang, D., Xu, R., Mai, Z.-F., & Shao, L. 2023, *Phys. Rev. D*, 107, 044053, doi: [10.1103/PhysRevD.107.044053](https://doi.org/10.1103/PhysRevD.107.044053)
- Luo, J., Chen, L.-S., Duan, H.-Z., et al. 2016, *Classical and Quantum Gravity*, 33, 035010, doi: [10.1088/0264-9381/33/3/035010](https://doi.org/10.1088/0264-9381/33/3/035010)
- Macedo, C. F. B., Pani, P., Cardoso, V., & Crispino, L. C. B. 2013, *The Astrophysical Journal*, 774, 48, doi: [10.1088/0004-637X/774/1/48](https://doi.org/10.1088/0004-637X/774/1/48)
- Merritt, D. 2004, *Phys. Rev. Lett.*, 92, 201304, doi: [10.1103/PhysRevLett.92.201304](https://doi.org/10.1103/PhysRevLett.92.201304)
- Merritt, D., Milosavljević, M., Verde, L., & Jimenez, R. 2002, *Phys. Rev. Lett.*, 88, 191301, doi: [10.1103/PhysRevLett.88.191301](https://doi.org/10.1103/PhysRevLett.88.191301)
- Navarro, J. F., Frenk, C. S., & White, S. D. M. 1996, *ApJ*, 462, 563, doi: [10.1086/177173](https://doi.org/10.1086/177173)
- Navarro, J. F., Frenk, C. S., & White, S. D. M. 1997, *The Astrophysical Journal*, 490, 493, doi: [10.1086/304888](https://doi.org/10.1086/304888)
- Nishikawa, H., Kovetz, E. D., Kamionkowski, M., & Silk, J. 2019, *Phys. Rev. D*, 99, 043533, doi: [10.1103/PhysRevD.99.043533](https://doi.org/10.1103/PhysRevD.99.043533)
- Press, W. H. 1977, *Phys. Rev. D*, 15, 965, doi: [10.1103/PhysRevD.15.965](https://doi.org/10.1103/PhysRevD.15.965)
- Ruan, W.-H., Liu, C., Guo, Z.-K., Wu, Y.-L., & Cai, R.-G. 2020, *Nature Astron.*, 4, 108, doi: [10.1038/s41550-019-1008-4](https://doi.org/10.1038/s41550-019-1008-4)
- Sadeghian, L., Ferrer, F., & Will, C. M. 2013, *Phys. Rev. D*, 88, 063522, doi: [10.1103/PhysRevD.88.063522](https://doi.org/10.1103/PhysRevD.88.063522)
- Sago, N., & Fujita, R. 2015, *Progress of Theoretical and Experimental Physics*, 2015, 073E03, doi: [10.1093/ptep/ptv092](https://doi.org/10.1093/ptep/ptv092)
- Schumann, M. 2019, *Journal of Physics G: Nuclear and Particle Physics*, 46, 103003, doi: [10.1088/1361-6471/ab2ea5](https://doi.org/10.1088/1361-6471/ab2ea5)
- Shen, Z.-Q., Yuan, G.-W., Jiang, C.-Z., et al. 2023, Exploring dark matter spike distribution around the Galactic centre with stellar orbits. <https://arxiv.org/abs/2303.09284>
- Speeney, N., Antonelli, A., Baibhav, V., & Berti, E. 2022, *Phys. Rev. D*, 106, 044027, doi: [10.1103/PhysRevD.106.044027](https://doi.org/10.1103/PhysRevD.106.044027)
- Tang, M., Xu, Z., & Wang, J. 2021, *Chinese Physics C*, 45, 015110, doi: [10.1088/1674-1137/abc680](https://doi.org/10.1088/1674-1137/abc680)
- Traykova, D., Clough, K., Helfer, T., et al. 2021a, *Phys. Rev. D*, 104, 103014, doi: [10.1103/PhysRevD.104.103014](https://doi.org/10.1103/PhysRevD.104.103014)
- . 2021b, *Phys. Rev. D*, 104, 103014, doi: [10.1103/PhysRevD.104.103014](https://doi.org/10.1103/PhysRevD.104.103014)
- Traykova, D., Vicente, R., Clough, K., et al. 2023, *Phys. Rev. D*, 108, L121502, doi: [10.1103/PhysRevD.108.L121502](https://doi.org/10.1103/PhysRevD.108.L121502)
- Virtanen, P. e. a. 2020, *Nature Methods*, 17, 261–272, doi: [10.1038/s41592-019-0686-2](https://doi.org/10.1038/s41592-019-0686-2)
- Yue, X.-J., & Cao, Z. 2019, *Phys. Rev. D*, 100, 043013, doi: [10.1103/PhysRevD.100.043013](https://doi.org/10.1103/PhysRevD.100.043013)
- Yue, X.-J., & Han, W.-B. 2018, *Phys. Rev. D*, 97, 064003, doi: [10.1103/PhysRevD.97.064003](https://doi.org/10.1103/PhysRevD.97.064003)
- Yue, X.-J., Han, W.-B., & Chen, X. 2019, *The Astrophysical Journal*, 874, 34, doi: [10.3847/1538-4357/ab06f6](https://doi.org/10.3847/1538-4357/ab06f6)
- Zhang, C., Fu, G., & Dai, N. 2024, Detecting dark matter with extreme mass-ratio inspirals. <https://arxiv.org/abs/2401.04467>
- Zhao, H., & Silk, J. 2005, *Phys. Rev. Lett.*, 95, 011301, doi: [10.1103/PhysRevLett.95.011301](https://doi.org/10.1103/PhysRevLett.95.011301)